A Platinum Open Access Journal for Organic Chemistry

Paper

Free to Authors and Readers | DOAJ Seal | *Arkivoc* **2024** (3) 202312162

Hydrogenation of cinnamaldehyde over palladium nanoparticles supported on functionalized N-doped solid carbon spheres

Alice Magubane[a,b,c], Manoko S. Maubane-Nkadimeng,[a,b,d] and Neil J. Coville[a,b*]

[a] DSI-NRF Centre of Excellence in Strong Materials, University of the Witwatersrand, Johannesburg 2050, South Africa; [b] Molecular Sciences Institute, School of Chemistry, University of the Witwatersrand, Johannesburg 2050, South Africa; [c] Institute of Catalysis and Energy Solutions, University of South Africa, Florida Campus, Johannesburg 1710, South Africa; [d] Microscopy and Microanalysis Unit, University of the Witwatersrand, Johannesburg, South Africa

Email: neil.coville@wits.ac.za

We wish to dedicate this paper to Professor Graham Hutchings in recognition of his contributions to catalysis over many decades. A successful career that has not ended yet.

Received 12-28-2023 **Accepted Manuscript** 03-24-2024 **Published on line** 03-27-2024

Abstract

Selective hydrogenation of the C=O bond, rather than the conjugated C=C bond, in cinnamaldehyde (CALD) is still an interesting challenge. Herein, Pd catalysts supported on solid carbon spheres (SCSs) and functionalized solid carbon spheres (fSCSs) were explored for the selective hydrogenation of CALD. The Pd/fSCSs catalyst (Pd wt.% 3.7) gave cinnamyl alcohol (CA) selectivity of 85% and CALD conversion of 99% (6 h at T = 60 °C), while the Pd/SCSs catalyst (Pd wt.% 3.6) gave 100% CALD conversion (4 h, 100% selectivity) towards 3-phenyl-1-propanol. The Pd/fSCSs catalyst unfortunately showed poor stability in repeat reactions.

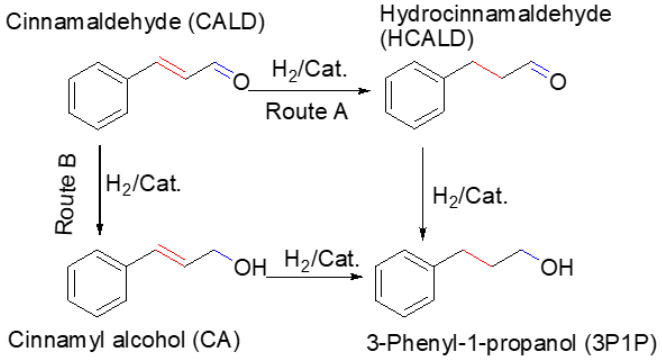

Keywords: Solid carbon spheres; hydrogenation; palladium; cinnamaldehyde; cinnamyl alcohol

Cite as *Arkivoc* **2024** (3) 202312162
DOI: https://doi.org/10.24820/ark.5550190.p012.162

Introduction

Chemoselective hydrogenation of α,β-unsaturated aldehydes is an important reaction, both from an academic and industrial point of view. This reaction is used in the production of fine chemicals, spices, and pharmaceutical intermediates.[1–3] One of the model reactions for the study of these types of reactions with α,β-unsaturated aldehydes is cinnamaldehyde (CALD). The immense interest in the selective hydrogenation of CALD arises because: (i) the products produced in this reaction are of economic value in both the pharmaceutical and fragrance industries, and (ii) conjugation exists between the C=C bond and C=O bond in CALD which impacts on their chemistry.[1,4,5] The selective hydrogenation of CALD can occur through different pathways (scheme 1): via hydrogenation of the C=C bond to form hydrocinnamaldehyde (HCALD) or hydrogenation of the C=O bond to form cinnamyl alcohol (CA). Both HCALD and CA can be further hydrogenated to form 3-phenyl-1-propanol (3P1P).[1–3] The reduction of the C=C bond compared to C=O bond is thermodynamically and kinetically favoured.[4,6,7]

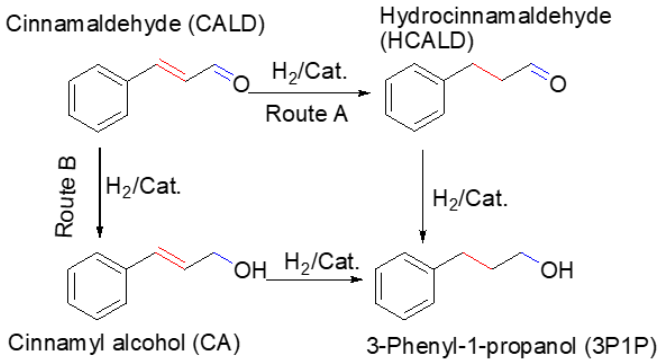

Scheme 1. Reaction pathway for the selective hydrogenation of CALD.

Numerous supported noble metals (i.e., Au, Pd, Pt, Ru, and Ir) and non-noble metals (i.e., Fe, Co, and Ni) have been used for the selective hydrogenation of CALD.[5,8–10] Research work has shown that Pt, Ir, Co, Ru and Au are typically more selective for the hydrogenation of the C=O bond than Pd, Cu and Ni.[8–10] Indeed, Pd is a classical C=C bond hydrogenation catalyst.[11–13] Various factors such as metal particle size, solvent effects, and catalyst support properties can also influence the selectivity and activity of the reaction and change the expected reaction product.[2,14,15]

One of the ways used by researchers to enhance the catalyst selectivity and activity in the selective hydrogenation of CALD to CA is by modifying the electronic properties of the catalyst.[14,16,17] This can be done by placing the metal on different supports; different metal-support interactions will influence the course of the reaction. Carbon nanomaterials (CNMs) are one example of a support that has been used to enhance the rate of many catalytic reactions by influencing the electron transfer from the CNM to the metal active site.[2,16] The surface chemical properties of CNMs have been reported to favour the adsorption of organic compounds with weak polarity on its surface resulting in an enhanced catalyst reaction rate.[2,16,18,19] Metals supported on CNMs such as carbon nanotubes (CNTs), carbon nanofibers (CNFs), activated carbon (AC), graphene and graphene oxide have all been used as catalyst supports in the selective hydrogenation of CALD.[2,11,18,20]

In particular, Pd supported on CNMs has been shown as a promising catalyst for the selective hydrogenation of CALD. Studies have reported on the role of the metal deposition and activation method,[12] carbon support

surface chemistry,[2,11,21] N dopants,[22] poison tolerance,[20] confinement effect[23] and solvent effect[18] on the selectivity and activity of Pd supported on different CNMs.

Importantly, reports have indicated that the presence of polar functional groups on the carbon support can alter the selectivity and activity of a catalyst (e.g., by reducing the CALD adsorption on the metal surface by interactions with the phenyl group).[1,24] Zeng *et al.* investigated the effect of a pre-treated AC support on the activity and selectivity of Pt NPs in the hydrogenation of CALD.[1] The AC was pre-treated with different concentrations of KOH under microwave radiation. The enhancement in the selectivity to CA was attributed to the increase in the oxygen-containing functional groups on the surface of the support. It was proposed that the oxygen-containing functional groups reduced the CALD adsorption mode via interaction with the benzene ring, which reduced the distance of the C=O bond from the metal surface.

Herein we report on the liquid phase selective hydrogenation of CALD as a model reaction to study the effect of the surface chemistry of acid functionalized solid carbon spheres (fSCSs) when used as a support for a Pd catalyst. SCSs are an easy to make carbon material that can be made in large quantities and with varying sizes, doped with nitrogen, and containing different surface functional groups. In this study the SCSs were treated with nitric and sulfuric acid to give fSCSs and the prepared catalyst was compared to a Pd/SCSs catalyst. Acid treatment of CNMs has been reported to enhance the interaction between the support and the metal due to the presence of defects and oxygenated groups.[1,25] The Pd/SCSs catalyst favoured the complete hydrogenation of CALD forming 3P1P, whereas the Pd/fSCSs catalyst produced CA, and not HCALD, as a major product. The results from the study suggest that the use of ethanol, the Pd particle size and the presence of the oxygen-containing functional (and possibly N-doping) groups on the fSCS all contributed to the selectivity of the Pd/fSCSs catalyst.

Results and Discussion

The characterization results for the synthesized carbon supports were consistent with data from other literature reports and are hence only reported in the supplementary information.[28]

Characterization of Pd/SCSs and Pd/fSCSs

TEM analysis

Figure 1 shows the TEM images of the Pd/SCSs and Pd/fSCSs and their corresponding Pd particle size distribution. The TEM images (Figure 1a and 1b) show that the Pd particles are dispersed on the surface of the carbon spheres, and some agglomeration of the Pd particles (circled in yellow) was observed on both supports. The average particle size of the Pd particles supported on SCSs and fSCSs was determined to be 6.0 ± 2.3 and 12.0 ± 3.4 nm respectively (see Figure 1c). The Pd particles supported on the SCSs have a narrow particle size range distribution (2-11 nm) as opposed to the Pd on the fSCSs support (4-24 nm). This variation can be ascribed to the difference in the oxygen content of the supports (see section 3.1.5). In the literature, a low oxygen content on a carbon support has been reported to favour the formation of well dispersed Pd NPs (particle size < 3 nm) when using a Pd chloride precursor.[26] This is because of the weak adsorption capacity of the Pd chloride precursor on the surface carbon support with a low oxygen content.[26,27]

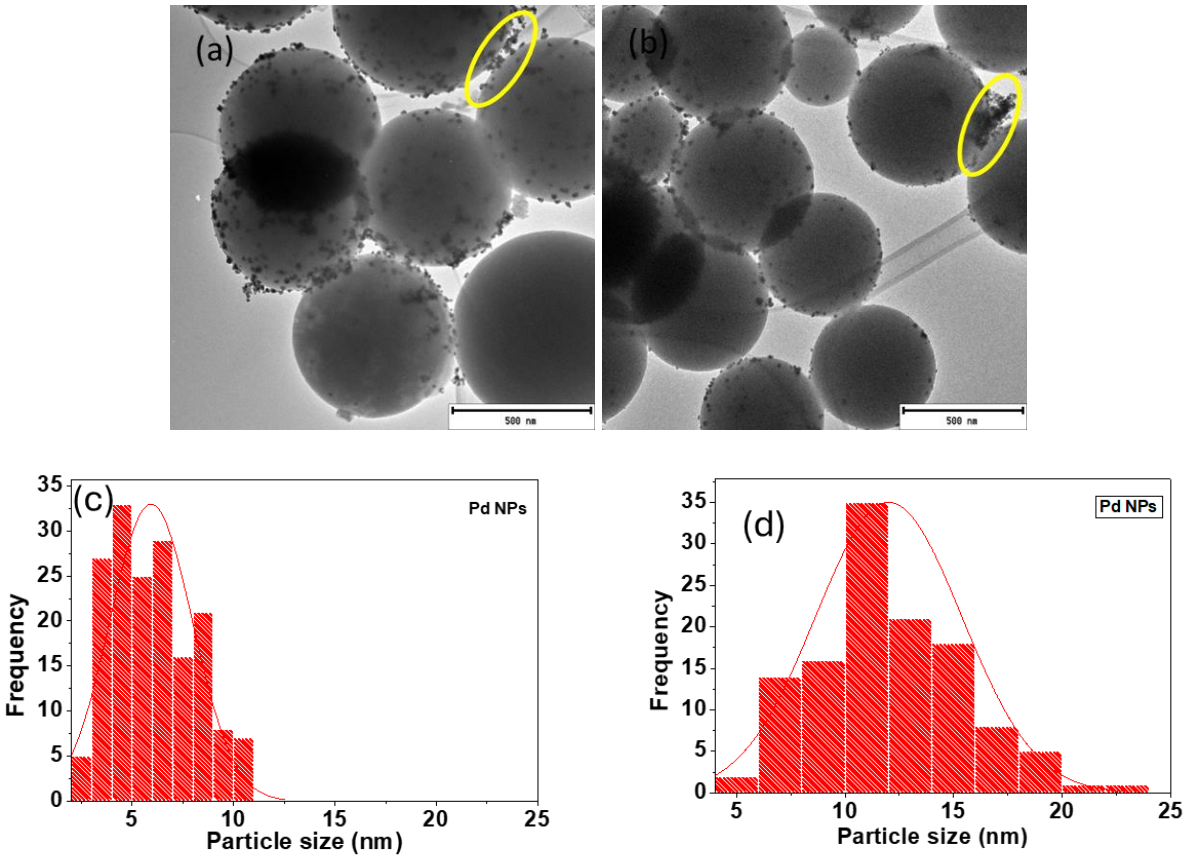

Figure 1. TEM images images of (a) Pd/SCSs and (b) Pd/fSCSs, and their corresponding (c and d) particle size distributions.

Thermogravimetric analysis

The percentage loading of Pd on the carbon supports was determined using the TGA technique. The TGA and DTG profiles of Pd/SCSs and Pd/fSCSs are shown in Figure 2a and 2b respectively. The metal residues (as PdOx) left after the decomposition of the carbon supports in an oxidative environment (air) were estimated to be 4.2% and 4.3% for the two catalysts to give Pd loadings of 3.6% (Pd/SCSs) and 3.7% (Pd/fSCSs). The Pd NPs on the carbon supports catalyzed the oxidation of the carbon as shown by a decrease in the weight-loss temperature of the carbon.[28] For the Pd/SCSs catalyst, the carbon weight-loss temperature decreased from *ca.* 653 °C to 512 °C, while for the Pd/fSCSs catalyst it decreased from *ca.* 608 °C to 469 °C when compared to the non-metal containing supports (Figure S2a and S2b). The rapid loss of mass due to the Pd is due to the catalyzed carbon reaction. A large moisture-loss peak (13.3 wt.%) can be seen for the Pd/fSCSs catalyst at *ca.* 100 °C, due to the presence of polar surface functional groups on the support. The Pd/fSCSs DTG profile, also showed additional peaks at c*a.* 226 °C and 340 °C which can be attributed to the loss of the carbon-containing functional groups (10.6 and 4.5 wt.% respectively).

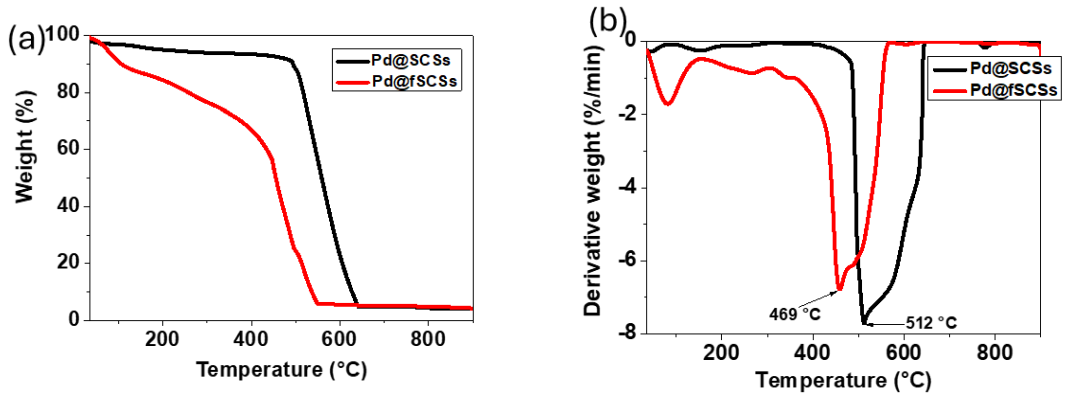

Figure 2. (a) TGA and (b) DTG profiles for air-oxidation of Pd/SCSs and Pd/fSCSs.

BET analysis

Table 1 summarizes the surface analyses of the carbon supports and the catalysts, along with the percentage loadings of Pd and average particle/crystallite size of Pd. The BET surface area of the Pd supported on SCSs decreased, presumably due to blockage of the pores of the SCSs.[2]

Table 1. Properties of the carbon supports and of the catalyst supported on the carbon spheres

Sample	TEM Pd particle size (nm)	XRD Pd crystallite size (nm)	% Pd TGA	BET surface area (m^2/g)	Pore size (nm)	Pore volume (cm^3/g)
SCSs	-	-	-	557	2.3	0.32
Pd/SCSs	6.0 ± 2.3	6.7	3.6	390	2.4	0.23
fSCSs	-	-	-	531	2.3	0.30
Pd/fSCSs	12.0 ± 3.4	8.9	3.7	573	2.4	0.35

PXRD analysis

To confirm that the reduced Pd NPs were in the metallic phase, the two catalysts were analyzed using PXRD (Figure 3). The PXRD pattern of the Pd/SCSs and Pd/fSCS showed five peaks at 2Θ values of 40.5°, 46.9°, 68.5°, 82.3° and 86.9° which corresponds to Pd nanoparticle crystal planes: (111), (200), (220), (311) and (222) [PDF 00-001-1201]. The Pd crystallite size was estimated using the Scherrer equation. The most intense peak of the diffraction pattern corresponding to the (111) plane was used to calculate the crystallite size of the Pd, and the values obtained were 6.7 nm and 8.9 nm for the Pd/SCSs and Pd/fSCSs respectively. The difference in the PXRD and TEM values can be ascribed to the different particle size measurements (Table 1). The PXRD estimation is solely based on the diffracting crystallite planes and not the whole particles. No noticeable shift of the carbon peak was observed.

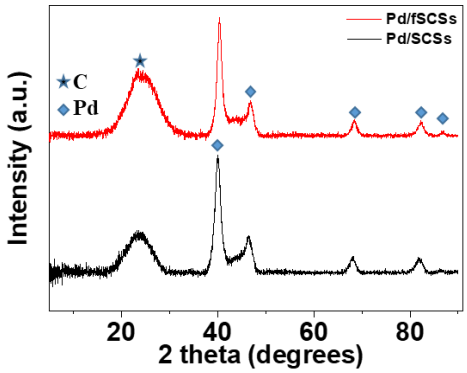

Figure 3. PXRD profiles of the Pd/SCSs and Pd/fSCSs.

XPS analysis

Figure 4 (a and b) shows the XPS spectra of the Pd/SCSs and Pd/fSCSs catalysts. The XPS spectra of the catalysts, when compared to the fSCSs support before Pd loading (Figure S5a), show additional peaks for Pd 3d (335.3 and 335.5 eV) for the Pd/SCSs and Pd/fSCSs respectively. The deconvolution of the C1s XPS spectrum (Fig. 4c, d) of the Pd/SCSs and Pd/fSCSs catalysts respectively, shows 5 types of carbon species with peaks in the spectrum that correspond to C-C sp^2 (284.2 eV), C-C sp^3 (284.6 and 284.8 eV), C-O (285.8 eV), C=O (288.0 eV) and O-C=O (290.0 and 289.8 eV). The deconvolution of O1s spectra (Figure S7) shows the presence of the Pd-O, *viz*. O1s (C-O; Pd oxide) and O1s ((C=O), Pd 3p oxide), with the binding energy of (531.7 and 532.7 eV) and (531.2 and 532.8 eV) for Pd/SCSs and Pd/fSCSs catalysts respectively. The XPS data of both the catalysts showed that the electronic properties of Pd remained relatively the same, regardless of the support used.

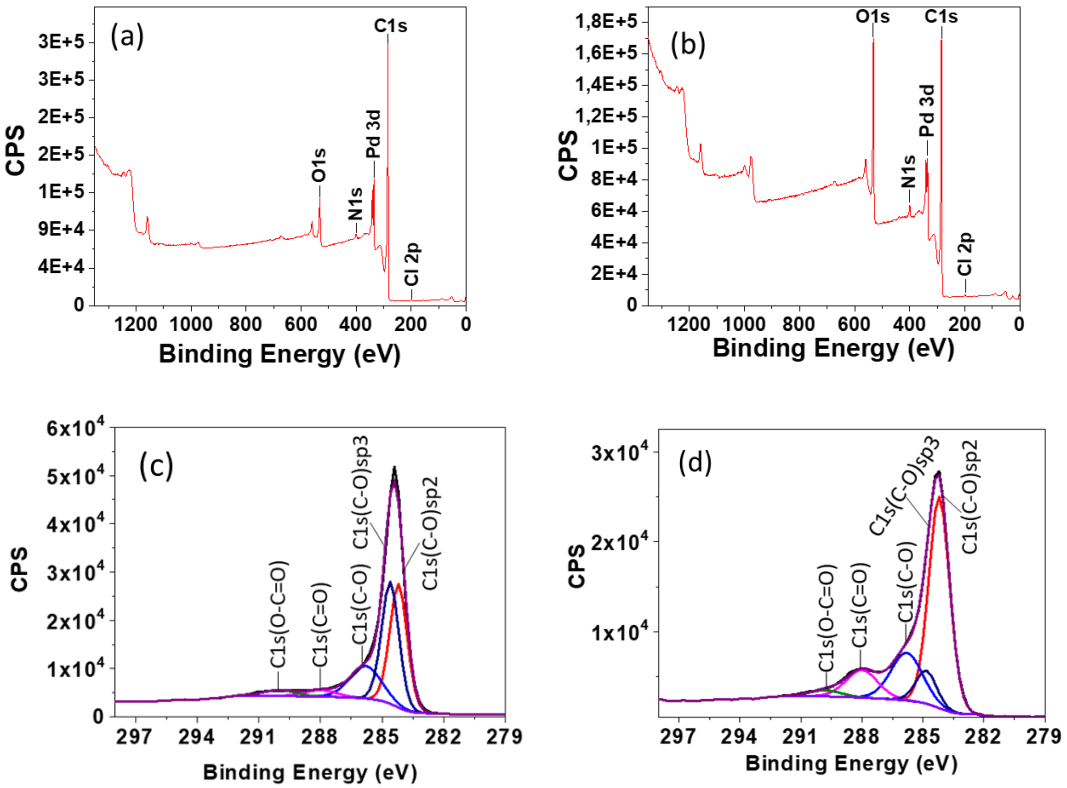

Figure 4. (a and b) XPS spectra and (c and d) C1s spectra of Pd/SCSs and Pd/fSCSs catalysts respectively.

Table 2 summarizes the XPS elemental quantification of Pd/SCSs and Pd/fSCSs. From the data it can be noted that the C1s atomic % decreased from 87.6% to 72.4% and the O1s content increased from 8.7% to 22.6% after functionalization of the carbon spheres. Part of the change in the atomic % of O1s is probably due to the variation in PdOx content associated with surface oxidation of Pd on the supports. Both the carbon supports showed the presence of N which can be attributed to acid (HNO_3) treatment of the carbon spheres,[29] while the small Cl content could be due to residual Cl from the Pd salt used.

Table 2. Elemental quantification of Pd/CSs catalysts using XPS analysis

Catalyst	Elemental composition (atomic %)				
	C1s	O1s	N1s	Pd 3d	Cl 2p
Pd/SCSs	87.6	8.7	1.2	2.3	0.2
Pd/fSCSs	72.4	22.6	2.6	2.2	0.2

Table 3 summarizes the relative % content of the Pd^0 and Pd oxide species present in both catalysts. The surface content of Pd^0 species was estimated to be 76% and 68% for Pd/SCSs and Pd/fSCSs catalysts respectively. From the data obtained, it can be noted that the surface of the Pd/fSCSs catalyst is more oxidized and hydrophilic (presence of more oxygenated functional groups on the support) and, also contains more nitrogen. A similar trend was also observed from the study reported by Xu *et al.* in which they reported the content of Pd^0 species of 73.1% and 61.6% for Pd supported on graphite felt (GF) and oxygen functionalized graphite felt (OGF) respectively.[12] The BE of Pd^0 in both the catalysts is slightly different (± 0.2 eV), and may imply that the degree of metal-support interaction is different.[26]

Table 3. Binding energy and % of Pd, PdO, and PdO_2 content of the Pd/CSs catalysts from XPS

Catalyst	BE (eV) Pd $3d_{5/2}$	Pd %	PdO %	PdO_2 %	Pd^{2+}/Pd^0
Pd/SCSs	335.2	76	14	10	0.18
Pd/fSCSs	335.0	68	16	16	0.24

The XPS data for the nitrogen peaks are given in Table S1.

Hydrogenation of CALD

The selective hydrogenation of CALD was carried out in a liquid phase reaction over the Pd/fSCSs and Pd/SCSs catalysts. The CALD reaction was studied using different reaction conditions including temperature, H_2 gas flow rate, stirring rate, catalyst mass and concentration. The reaction conditions used were established from various preliminary studies and literature reports.[30] A comparison between the catalytic activity of the Pd/fSCSs and Pd/SCSs catalysts was made. A blank test (hydrogenation in the presence of fSCSs or SCSs) was carried out in the absence of Pd and no catalytic activity was observed.

Optimization of conditions

Catalyst selectivity

Ethanol was chosen as the solvent for the study, as reports have indicated that this is the solvent that has the most potential for generating the CA product.[30] The catalyst activities of Pd/SCSs and Pd/fSCSs for the hydrogenation of CALD were compared (reference conditions: 6 h, 100 mg catalyst, 50 mL/min = H_2 flow rate, 100 mL ethanol, T = 60 °C and 1.32 g CALD). Under these conditions, the Pd/SCSs gave 100% selectivity to 3P1P i.e., total hydrogenation of both C=C and C=O bonds (Figure 5; Table 4). This outcome can arise from various factors. In comparison, the Pd/fSCSs catalyst gave predominantly CA, i.e. a preferential reduction of the C=O bond. In the literature, it has been reported that if the Pd particle size (> 3 nm) is small both the CALD C=C and C=O bonds become readily accessible to the metal surface and can be hydrogenated. For example, Jiang *et al.* studied the effect of particle size of supported Pd NPs (size range of 1-6 nm) on CALD hydrogenation.[31] These authors reported that Pd NPs with sizes less than 3 nm had higher selectivity (over 90%) towards HCALD and when Pd NPs with the size of 5.7 nm was used the catalyst selectivity towards HCALD decreased (77.5%). As the Pd NPs size increased over-hydrogenation of CALD was noted (3P1P selectivity 1.3 nm: 4.3% and 5.7 nm: 22.5%).

A similar effect has been proposed for the adsorption of CALD on a Pd (111) plane. Thus, the selectivity of the Pd/fSCSs to the CA product can be linked to the particle size (12 nm) and the presence of more Pd (111) planes.[11,31] Pd/fSCSs catalyst selectivity toward CA, can also be ascribed to oxygen-containing functional groups. Zeng *et al.* proposed that the oxygen-containing functional groups reduced the CALD adsorption mode via the benzene ring which reduced the distance of the C=O bond from the metal surface.[1] The XPS and TGA data clearly indicate the large amount of surface functional groups on the fSCSs. This suggest that the functional groups impact on the Pd catalytic behaviour.

The impact of the N-doping on the selectivity is not clear. Most literature reports suggest that N-doped carbons lead to better metal dispersion in metal/carbon support catalysts. However, in this study the Pd particle size increased while the N-doping increased, suggesting that the oxygen doping played the more significant role in the reaction.

Table 4. CALD conversion and selectivity of Pd/fSCSs and Pd/SCSs

Sample	CALD conversion %	Selectivity (%)			
		CA	3P1P	HCALD	Other
Pd/fSCSs	98.7	92.33	3.33	0	4.34
Pd/SCSs	100	0	100	0	0

Reference conditions: 4 h, 100 mg catalyst, 50 mL/min = H_2 flow rate, 100 mL ethanol, T = 60 °C, and 1.32 g CALD.

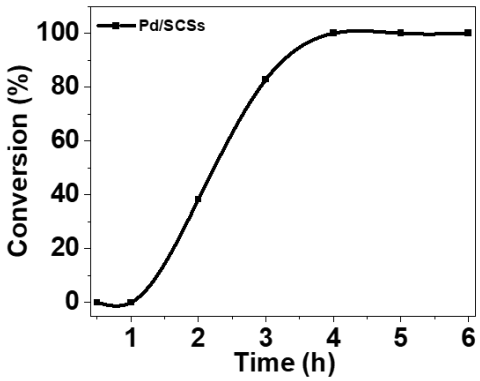

Figure 5. Conversion of CALD over Pd/SCSs. Reference conditions: 6 h, 100 mg catalyst, 50 mL/min = H_2 flow rate, 100 mL ethanol, T = 60 °C, and 1.32 g CALD.

As the Pd/SCSs catalyst over-hydrogenated the CALD, only the Pd/fSCSs catalyst was further evaluated in the CALD hydrogenation.

Influence of reaction temperature

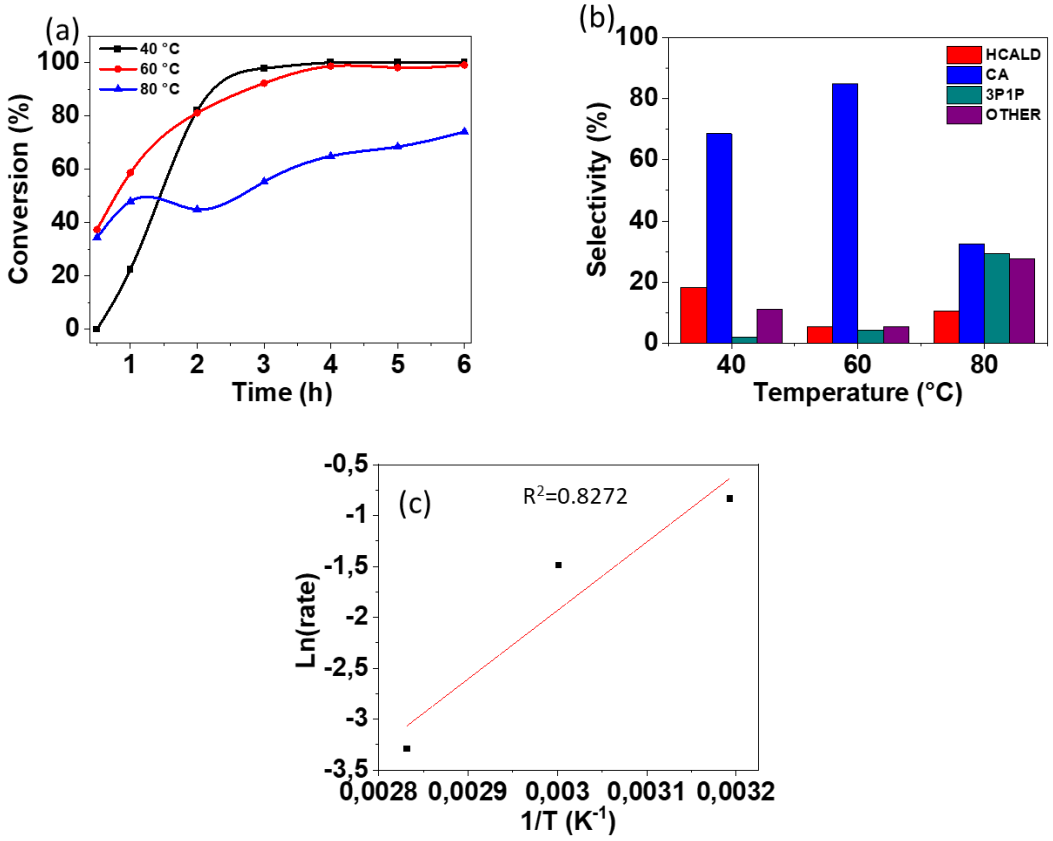

Figure 6. The influence of temperature on the (a) CALD conversion and (b) selectivity, and (c) Arrhenius plot for CALD hydrogenation over the Pd/fSCSs. Reference conditions: 6 h, 100 mg catalyst, 50 mL/min = H_2 flow rate, 100 mL ethanol, and 1.32 g CALD.

Figure 6a shows the influence of the reaction temperature on the activity and selectivity of the Pd/fSCSs catalyst on the hydrogenation of CALD. It can be noted that CALD conversion decreased with an increase in temperature. This observation can be ascribed to CALD over-hydrogenation to produce by-products that poison the catalyst.[1] The by-products formed can include acetals formed due to condensation of CALD/HCALD with ethanol and β-methyl styrene due to a side reaction with CA, which can be further reduced to propyl benzene.[32] In terms of selectivity, this catalyst was more selective to C=O bond hydrogenation, forming CA, but all three products (CA, HCALD, and 3P1P) and other 'extra' products (Figure 6b) were detected by GC. The optimum temperature was 60 °C in terms of both activity and selectivity (i.e., hydrogenation of the C=O bond).

Figure 6c shows the Arrhenius plot for the hydrogenation of CALD catalyzed using the Pd/fSCSs catalyst. The Arrhenius plot was used to determine the activation energy of the catalyst that was calculated to be 56 kJ/mol. This value is comparable to the value (70 kJ/mol) reported by Cabiac *et al.* for the hydrogenation of CALD using 4 wt.% Pd/AC catalysts using cyclohexane as a solvent.[33]

Influence of catalyst loading

The influence of the Pd/fSCSs catalyst amount on the conversion of CALD was studied while keeping the temperature (60 °C) and H_2 flow rate (50 mL/min) constant. Figure 7a shows the conversion of CALD over varying amounts of catalyst. From the data obtained it can be noted that when using 50 mg catalyst the lowest CALD conversion of 65.8% was obtained after 6 hours. Increasing the catalyst mass (100-200 mg) increased the CALD conversion (99% to 100%). The catalyst selectivity towards CA increased from the use of 50 to 100 mg catalyst and then decreased with an increase in the catalyst mass (Figure 7b). The use of a larger catalyst amount resulted in the over-hydrogenation of CALD forming 3P1P as a major product. This indicates that the reaction has now become controlled by diffusion effects combined with reaction product poisoning effects. The data reveal that to obtain the maximum CA yield at the fastest rate, that the optimum catalyst loading for this study is 100 mg.

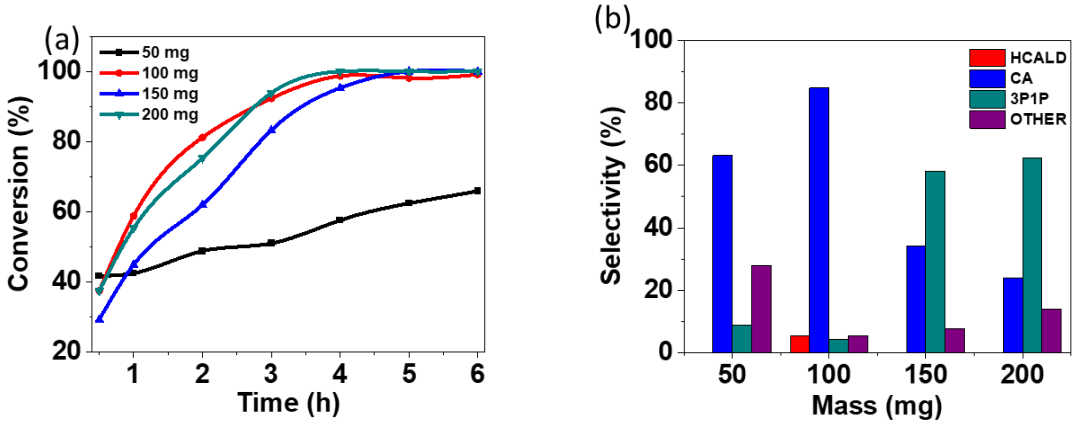

Figure 7. The influence of the Pd/fSCSs catalyst loading on the (a) CALD conversion and (b) selectivity. Reference conditions: 6 h, 50-200 mg catalyst, 50 mL/min = H_2 flow rate, 100 mL ethanol, T = 60 °C, and 1.32 g CALD.

Influence of H_2 gas flow rate

The catalytic activity of the Pd/fSCSs catalyst at different hydrogen flow rates is shown in Figure 8a. From the data presented, increasing the H_2 flow rate resulted in a moderate decrease in the conversion rate of the CALD. The results show that at a higher H_2 flow rate there is an increase in the adsorption of H_2 leading to (i) decreased adsorption of CALD and (ii) an increased possibility of over-reduction. The catalyst selectivity to CA decreased

from 85% to 45% and an increase in the formation of 3P1P, followed by other by-products was noted (Figure 8b).

The influence of O_2 on the CALD reaction was also investigated. This was achieved by not removing the dissolved oxygen with flowing N_2 gas before the CALD hydrogenation reaction was commenced (Figure 8c). Indeed, the traces of dissolved oxygen did have a minor impact on the hydrogenation of CALD. It is to be noted that the rate of CALD hydrogenation was reduced as observed by the decrease in the CALD conversion between 0.5 to 4 h. The reaction did go to completion (more slowly) indicating that any PdOx species were reduced in the reaction.

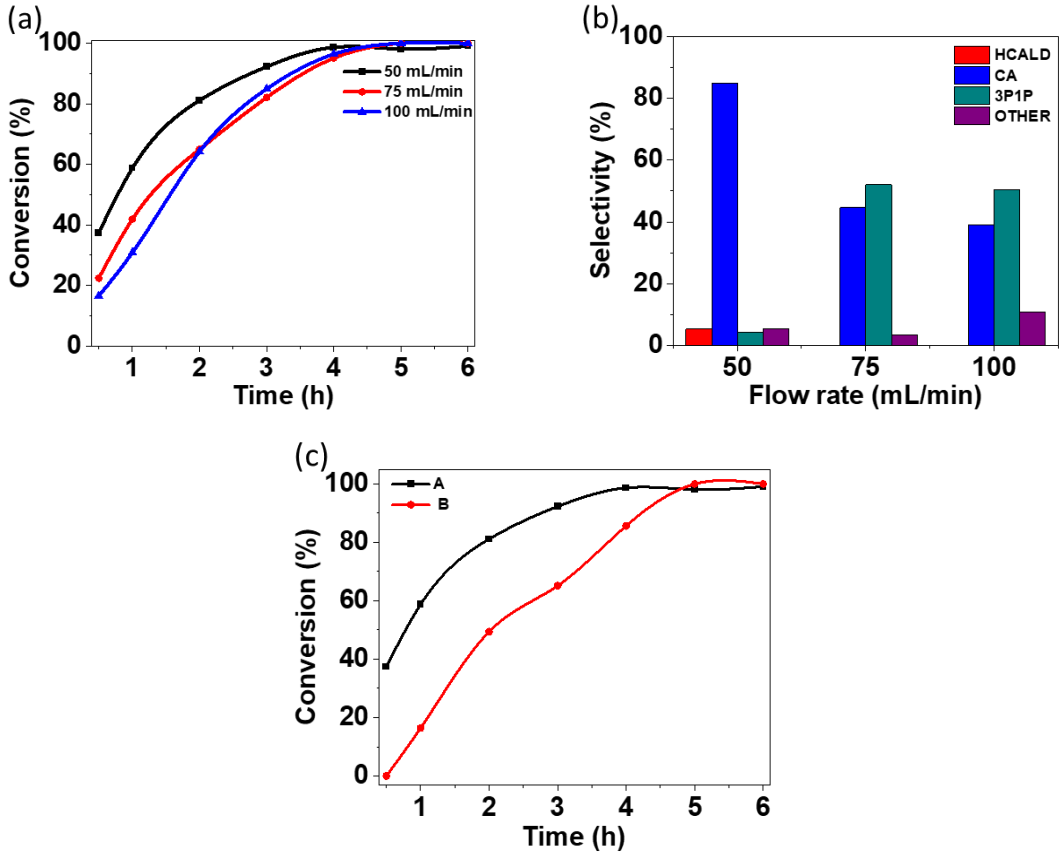

Figure 8. (a) The effect of H_2 flow rate on the (a) activity and (b) selectivity of the Pd/fSCSs catalyst, and (c) the effect of the removal of dissolved traces of oxygen (A: deoxygenated; (B): oxygenated) on the CALD conversion over the Pd/fSCSs catalyst. Reference conditions: 6 h, 100 mg catalyst, 50-100 mL/min = H_2 flow rate, 100 mL ethanol, T = 60 °C, and 1.32 g CALD.

Influence of CALD concentration

The effect of CALD concentration on the conversion and selectivity of the CALD reaction was measured at 60 °C, while keeping the catalyst mass (100 mg) and hydrogen flow rate (50 mL/min) the same (Figure 9). Increasing the CALD concentration from 0.05 M (0.66 g) to 0.1 M (1.32 g) resulted in a slight decrease in the reaction rate. This was unexpected. However, the selectivity data revealed the problem – the ability of the Pd to interact with both the CALD and H_2. At the lower CALD concentration, the reaction is rapid but secondary reactions occurred to give 3P1P, i.e. over-hydrogenation of CALD. At even higher concentrations, this effect became even more pronounced as the 'extra' products that formed, poisoned the catalyst.

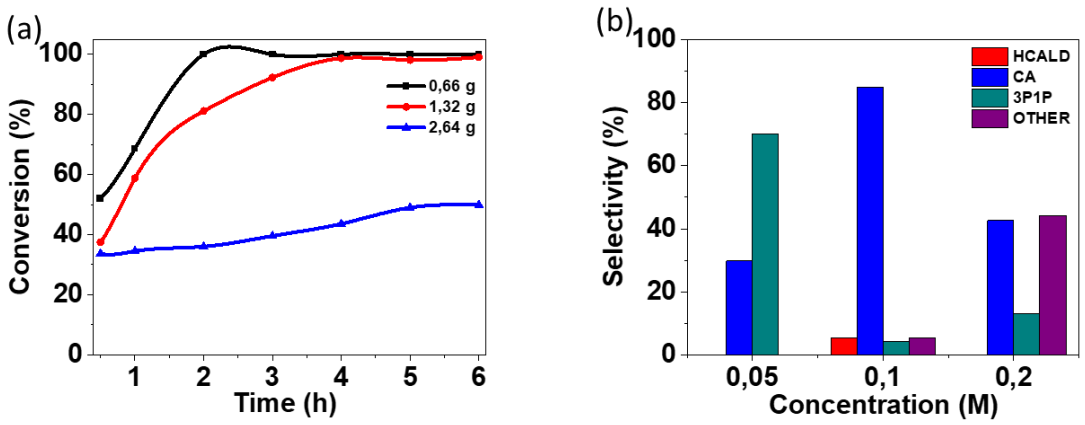

Figure 9. Effect of CALD concentration on the (a) conversion and (b) selectivity on the hydrogenation of CALD over the Pd/fSCSs catalyst. Reference conditions: 6 h, 100 mg catalyst, 50 mL/min = H_2 flow rate, 100 mL ethanol, T = 60 °C and 0.66-2.64 g CALD.

Influence of stirring rate

The hydrogenation of CALD was carried out at 60 °C with different stirring speeds (300, 600 and 900 rmp) and the results are shown in Figure 10a and 10b. It was observed that the CALD conversion occurred more rapidly with a stirring speed of 600 rmp. Even within half an hour, CALD conversions of 24%, 37% and 13% were obtained for stirring speeds of 300, 600, and 900 rmp respectively. The stirring rate appears to be influenced by two factors. At slow stirring speeds the catalyst-reactant interaction will occur slowly and the removal of product will be slow. This will lead to over-hydrogenated products. At very high stirring speeds the reaction will occur rapidly and over-hydrogenation can also occur leading to side products that are formed that poison the reaction. However, this proposal will need to be confirmed by further experiments.[12] The data parallel what was shown by the other variables. When the H_2 concentration was too low, a secondary reaction occurred and the selectivity to CA was poor. At higher H_2 concentrations the reaction is both faster and less over-reaction occurs. The optimum stirring speed of the three was thus 600 rmp.

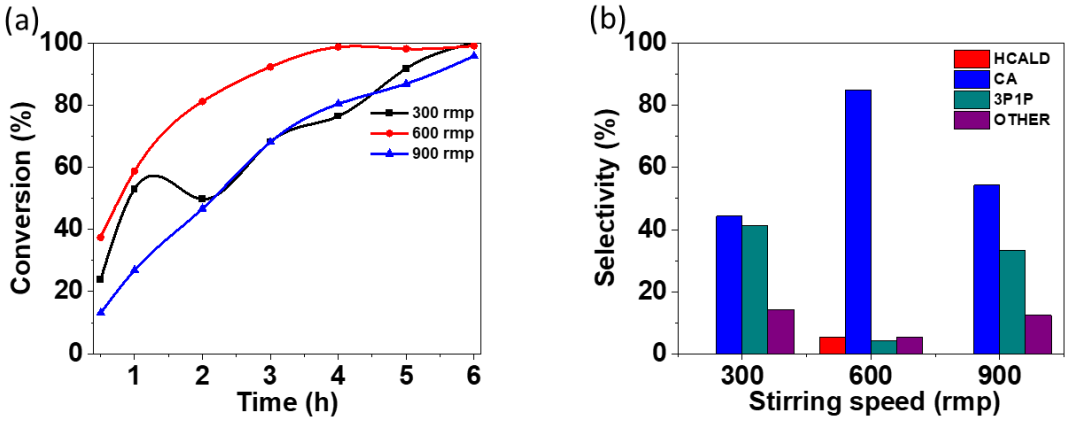

Figure 10. Influence of the stirring speed on (a) CALD conversion and (b) selectivity over the Pd/fSCSs catalyst. Reference conditions: 6 h, 100 mg catalyst, 50 mL/min = H_2 flow rate, 100 mL ethanol, T = 60 °C, and 1.32 g CALD.

Catalyst stability test

The stabilities of the Pd/fSCSs and Pd/SCSs catalysts were tested over five cycles while keeping the temperature (60 °C), CALD concentration (0.1 M), and H_2 flow rate (50 mL/min) constant. The catalyst performance and selectivity are shown in Figure 11a and 11b. The Pd/fSCSs catalyst maintained 100% CALD conversion after 6 h until cycle 3. The CALD conversion then decreased substantially during cycles 4 and 5 respectively. The Pd/SCSs catalyst maintained 100% CALD conversion throughout four runs. From cycles 4 and 5 the reaction rate started to slow down as shown by a decrease in the CALD conversion from 2 to 5 h; from the 5th cycle a maximum CALD conversion of 98% was obtained. The decrease in the catalyst activity can be ascribed to surface poisoning of the catalyst (due to over-hydrogenation of CALD) and Pd particle agglomeration on the surface of support. Figure S8 shows TEM images of spent catalysts with their corresponding particle size distributions. The Pd average particle increased from 6.0 ± 2.3 to 10.4 ± 4.8 nm for Pd/SCSs and 12.0 ± 3.4 to 17.6 ± 4.0 nm for Pd/fSCSs.

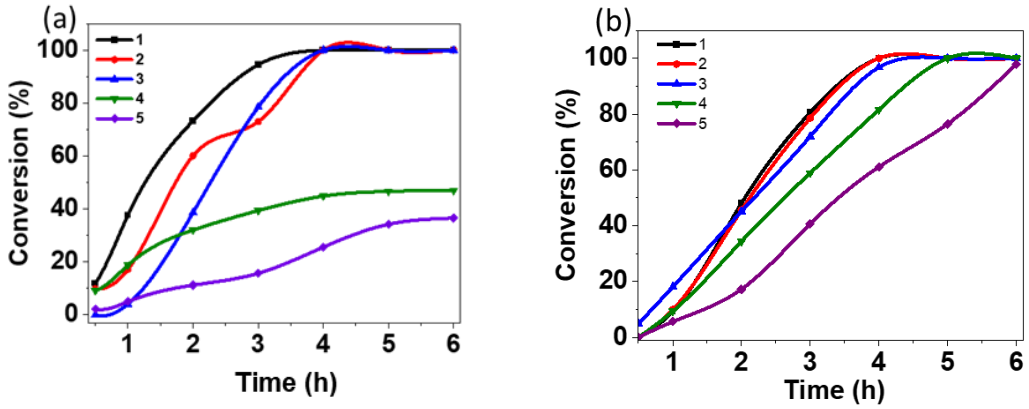

Figure 11. Recycling of (a) Pd/fSCSs and (b) Pd/SCSs over five cycles at 60 °C and 50 mL/min H_2 flow rate. Reference conditions: 6 h, initial catalyst mass= 100 mg, 50 mL/min = H_2 flow rate, 100 mL ethanol, T = 60 °C, and 1.32 g CALD.

Discussion

The Pd/fSCSs catalyst was used to study the selective hydrogenation of CALD. The product distribution of the catalyst varied depending on the reaction conditions used. In this study, the C=O bond was preferentially reduced, and CA was formed as a major product.

When the reaction temperature was increased (from 60 °C to 80 °C) the CALD conversion decreased from 99 to 74%. The formation of by-products can lead to the surface coverage of the active metal and, as a result, catalyst deactivation can occur.[1,20] CALD over-hydrogenation (i.e., reduction of both C=C and C=O bonds) occurred when the catalyst mass was increased (150 and 200 mg) and as a result the selectivity to CA decreased from 85 to 24%. A similar trend was observed when the hydrogen flow rate was increased (75 and 100 mL/min) and when a low concentration of CALD (0.05 M) was used.

The selectivity of the Pd/fSCSs catalyst to CA was unexpected as Pd metal is known to favour the reduction of the C=C bond of CALD resulting in the formation of HCALD.[2,12] However, the use of ethanol, the large Pd particle size, and the presence of polar functional groups on the surface of the carbon support can be used as an explanation for this observation.[1,34] It is not clear as to whether the nitrogen doping played an important role. Our data do not allow us to suggest which of these factors is the dominant one in the reaction that

determines the overall selectivity to the CA. Further, Vatti *et al.* studied the effect of intrinsic surface electropositive sites on supported Pd catalysts in the selective hydrogenation of CALD.[35] Among the catalysts tested the selectivity toward CA decreased in the following order 1% Pd/P25-TiO_2 > Pd/SiO_2 > Pd/ γ-Al_2O_3. The increase in the selectivity to CA was correlated to an increase in the Pd^{2+}/Pd^0 ratio. It was reported that the Pd^{2+} ions might act as Lewis sites which could act as preferential adsorption sites for the C=O bond.

The study opens up the possibility of modifying the CALD selectivity to alcohol formation via the use of SCSs. It is not clear as to whether this method will lead to catalysts with long lifetimes. However, the study rather suggests that modification of readily available carbon materials may be promising as a method to control the relative C=O/C=C reaction pathways. No attempt has been made to optimize the reaction, nor to attempt to extend the lifetime of the catalyst. This would require further studies.

Conclusions

In summary, SCSs were successfully synthesized through carbonization of RF resin spheres at 900 °C. Pd particles were successfully loaded on the SCSs and fSCSs. Larger Pd particles were obtained using the functionalized SCSs (*ca*. 12 nm) than the SCSs (*ca*. 6 nm). FTIR and XPS data showed that oxidation of the SCSs resulted in additional oxygen-containing functional groups being present. This was further supported by TGA data, in which the acid-treated SCSs showed additional peaks and early onset weight-loss temperature. The Pd 3d XPS spectra of the synthesized catalysts showed that the electronic properties of the Pd were relatively the same on both carbons, indicating that little change resulted from acid treatment of the SCSs. The Pd/SCSs and Pd/fSCSs catalysts were tested in the liquid phase hydrogenation of CALD. The use of the Pd/SCSs catalyst led to complete hydrogenation of the C=C and C=O bonds without formation of intermediate products. The Pd/fSCSs catalyst was found to be selective toward the reduction of the C=O bond, with some HCALD and 3P1P formation. The activity of the Pd/fSCSs catalyst decreased with an increase in the reaction temperature (60 to 80 °C). The formation of by-products was more pronounced at a reaction temperature of 80 °C. The stability of the catalysts was tested in five runs. The catalytic activity of Pd/fSCSs dropped after the 4th cycle from 100% CALD conversion to 47% and further went down to 37% on the fifth cycle. For the Pd/SCSs catalyst 100% CALD conversion was maintained until the 4th cycle.

Experimental Section

The method used to synthesize SCSs was modified from the method reported in the literature by Dlamini.[28]

General. The chemicals used were of technical and analytical grade. CALD (98%), CA (98%), 3P1P (98%, FCC), HCALD (90%) and $PdCl_2$ (99%) were purchased from Sigma-Aldrich. The absolute ethanol was purchased from MK chemical. HCl (32%), nitric acid (55%), and sulfuric acid (98%) were purchased from Associated Chemical Enterprise (PTY) LTD.

Synthesis of the solid carbon spheres. A 0.5 mL ammonia solution (25%) was added to an ethanolic solution made of distilled water (60 mL) and absolute ethanol (24 mL) and the solution was stirred for one hour. After an hour, a mass of 0.6 g resorcinol (R) was added, and the solution was stirred for 30 minutes. This was followed by the addition of 0.80 mL formaldehyde (F) and the mixture was then stirred for 24 h at room temperature. The mixture, inside a Schott bottle, was hydrothermally treated in an oil bath at 100 °C for 24 h. After

hydrothermal treatment, the reddish powder was recovered by centrifugation at 18000 rpm for 20 min, washed using ethanol and distilled water and then dried at 100 °C for 4 h. The RF resin spheres were carbonized at 900 °C for 4 h under nitrogen gas (20 mL/min) to obtain solid carbon spheres. The yield of the SCSs was calculated to be 42%.

Acid treatment of SCSs. The as-synthesized SCSs were functionalized using a standard acid treatment method.[29] A mass of 1 g of SCSs was added to a mixture of nitric acid (55%, 11.24 mL) and sulfuric acid (98%, 3.76 mL) in a 500 mL round bottom flask. The mixture was heated at reflux at 110 °C for 2 h. The acid treated SCSs were washed with distilled water until a pH of 7 was reached. The obtained fSCSs were oven-dried at 100 °C for 4 h.

Synthesis of 5 wt.% Pd/SCSs and Pd/fSCSs catalysts. The procedure for the impregnation of Pd NPs on the support was modified from the method reported by Zhu *et al.*[2]. A mass of 0.6 g carbon support was added to 141 mL of 2 mM H_2PdCl_4 solution, and the mixture was stirred overnight. A mass of 0.1895 g of sodium borohydride dissolved in ethanol was slowly added to the mixture with continuous stirring for 2 h to reduce the metal salt into metallic Pd NPs. The catalyst was filtered and washed using distilled water and absolute ethanol. The obtained black solid (Pd/fSCSs or Pd/SCSs) was oven-dried at 100 °C for 4 h.

Characterization techniques. The morphologies of the RF resin spheres, SCSs, and Pd/SCSs and Pd/fSCSs were analyzed by transmission electron microscopy (TEM; FEI Tecnai Spirit (T12) operating at 120 kV). The Pd particle size and spheres diameter were measured using Image J software by counting >100 particles from TEM images. The phase composition of the prepared samples was determined using a Bruker D2 phaser PXRD equipped with a Lynxene detector using Cu-Kα (λ = 1.54184 Å) radiation at 30 kV with a scan range from 5 ° ≤ 2Θ ≤ 90 ° in 0.026 steps. The thermal stability of the samples and catalyst loading were determined using a Perkin Elmer thermogravimetric analyzer (TGA 4000) in air in the temperature range of 35-900 °C (heating rate: 10 °C/min). A Micromeritics Tristar 3000 surface area and porosity analyzer was used to conduct N_2 adsorption-desorption experiments at -195 °C. Before analysis, the samples were degassed at 150 °C for 4 h under N_2 gas. The Raman spectra were recorded using a Bruker Senterra Raman spectrophotometer with a laser wavelength of 532 nm using Opus 7.1 software. The elemental composition of the samples was determined using X-ray photoelectron spectroscopy (XPS) using a Thermo ESCAlab 250Xi equipped with a monochromatic Al Kα X-ray source operating at 1486.7 eV.

Catalytic tests. The selective hydrogenation of CALD was carried out under atmospheric pressure in a three-neck round bottom flask (100 mL) equipped with a condenser, magnetic stirrer, gas inlet, and sampling port. The three-neck round bottom flask was placed inside an oil bath with a thermocouple to maintain the desired temperature. The reaction mixture consisted of 100 mg catalyst, 1.32 g CALD, and 100 mL absolute ethanol. To remove traces of dissolved oxygen, N_2 gas was bubbled into the reaction mixture while the temperature was ramped to 60 °C (2 °C/min). Once the oil bath reached 60 °C, N_2 gas was switched with H_2 gas (50 mL/min) to allow for hydrogenation of the CALD. The reaction was carried out for 6 h while taking samples of the reaction periodically for analysis.

Product analysis was carried out using an offline Varian 3700 GC with a flame ionization detector (FID) and a capillary column (Phenomenex Zebron, 30 m L. x 0.53 mm I.D. x 1.5 µ F.T.). The temperatures for the column, detector and injector were set to 300, 250, and 200 °C respectively, with N_2 (5 mL/min) as the carrier gas. Chemical standards (CALD, CA, HCALD, and 3-P1P) were used to identify the GC peaks, including spiking procedures to confirm the product identification.

Acknowledgements

We acknowledge the NRF, the DSI-NRF Centre of Excellence in Strong Materials (CoE-SM) and the University of the Witwatersrand (Postgraduate Merit Award) for funding.

Supplementary Material

Characterization of the carbon supports, and characterization of the catalysts are given in the supplementary material associated with this manuscript.

References

1. Zeng, L.; Yan, H.; Zeng, Y.; Li, Y.; Zhang, Z.; Liu, Z.; Liu, Z. *Can. J. Chem. Eng.* **2019**, *97*, 2505. https://doi.org/10.1002/cjce.23487
2. Zhu, J.; Dou, M.; Lu, M.; Xiang, X.; Ding, X.; Liu, W.; Li, M. *Appl. Catal. Gen.* **2019**, *575*, 11. https://doi.org/10.1016/j.apcata.2019.02.009
3. Zhang, L.; Chen, X.; Peng, Z.; Liang, C. *Mol. Catal.* **2018**, *449*, 14. https://doi.org/10.1016/j.mcat.2018.02.006
4. Hui, T.; Miao, C.; Feng, J.; Liu, Y.; Wang, Q.; Wang, Y.; Li, D. *J. Catal.* **2020**, *389*, 229. https://doi.org/10.1016/j.jcat.2020.05.036
5. Li, L.; Jiao, Z.-F.; Zhao, J.-X.; Yao, D.; Li, X.; Guo, X.-Y. *J. Catal.* **2023**, *425*, 314. https://doi.org/10.1016/j.jcat.2023.06.018
6. Führer, M.; Van Haasterecht, T.; Bitter, J. H. *Chem. Commun.* **2022**, *58*, 13608. https://doi.org/10.1039/D2CC05322E
7. Cui, R.; Zhou, J.; Wang, D.; Zhao, Y.; Xiang, X.; Shang, H.; Zhang, B. *Dalton Trans.* **2023**, *52*, 3325. https://doi.org/10.1039/D2DT03600B
8. Stucchi, M.; Manzoli, M.; Bossola, F.; Villa, A.; Prati, L. *Nanomaterials* **2021**, *11*, 362. https://doi.org/10.3390/nano11020362
9. Patil, K. N.; Manikanta, P.; Srinivasappa, P. M.; Jadhav, A. H.; Nagaraja, B. M. *J. Environ. Chem. Eng.* **2023**, *11*, 109168. https://doi.org/10.1016/j.jece.2022.109168
10. Martínez-Ortiz, M. J.; De La Rosa-Guzmán, M. A.; Vargas-García, J. R.; Flores-Moreno, J. L.; Castillo, N.; Guzmán-Vargas, A.; Morandi, S.; Pérez-Gutiérrez, R. M. *Can. J. Chem. Eng.* **2018**, *96*, 297. https://doi.org/10.1002/cjce.22946
11. Sairanen, E.; Karinen, R.; Borghei, M.; Kauppinen, E. I.; Lehtonen, J. *ChemCatChem* **2012**, *4*, 2055. https://doi.org/10.1002/cctc.201200344
12. Xu, Z.; Duong-Viet, C.; Liu, Y.; Baaziz, W.; Li, B.; Nguyen-Dinh, L.; Ersen, O.; Pham-Huu, C. *Appl. Catal. B Environ.* **2019**, *244*, 128. https://doi.org/10.1016/j.apcatb.2018.11.041
13. Nagpure, A. S.; Gurrala, L.; Gogoi, P.; Chilukuri, S. V. *RSC Adv.* **2016**, *6*, 44333. https://doi.org/10.1039/C6RA04154J

14. Bonita, Y.; Jain, V.; Geng, F.; O'Connell, T. P.; Ramos, N. X.; Rai, N.; Hicks, J. C. *Appl. Catal. B Environ.* **2020**, *277*, 119272. https://doi.org/10.1016/j.apcatb.2020.119272
15. Cao, Z.; Bu, J.; Zhong, Z.; Sun, C.; Zhang, Q.; Wang, J.; Chen, S.; Xie, X. *Appl. Catal. Gen.* **2019**, *578*, 105. https://doi.org/10.1016/j.apcata.2019.04.006
16. Li, Y.; Cheng, H.; Lin, W.; Zhang, C.; Wu, Q.; Zhao, F.; Arai, M. *Catal. Sci. Technol.* **2018**, *8*, 3580. https://doi.org/10.1039/C8CY00943K
17. Wang, X.; Liang, X.; Geng, P.; Li, Q. *ACS Catal.* **2020**, *10*, 2395. https://doi.org/10.1021/acscatal.9b05031
18. Lan, X.; Wang, T. *ACS Catal.* **2020**, *10*, 2764. https://doi.org/10.1021/acscatal.9b04331
19. Lamme, W. S.; Zečević, J.; de Jong, K. P. *ChemCatChem* **2018**, *10*, 1552. https://doi.org/10.1002/cctc.201701991
20. Chen, S.; Meng, L.; Chen, B.; Chen, W.; Duan, X.; Huang, X.; Zhang, B.; Fu, H.; Wan, Y. *ACS Catal.* **2017**, *7*, 2074. https://doi.org/10.1021/acscatal.6b02720
21. Zhang, Q.; Ma, Y.; Ma, J.; Meng, C.; Luo, S.; Liu, Y. *ACS Appl. Nano Mater.* **2023**, *6*, 8868. https://doi.org/10.1021/acsanm.3c01286
22. Abasabadi, R. K.; Khodadadi, A. A.; Mortazavi, Y. *Res. Chem. Intermed.* **2021**, *47*, 1429. https://doi.org/10.1007/s11164-020-04372-9
23. Tessonnier, J.-P.; Pesant, L.; Ehret, G.; Ledoux, M. J.; Pham-Huu, C. *Appl. Catal. Gen.* **2005**, *288*, 203. https://doi.org/10.1016/j.apcata.2005.04.034
24. Toebes, M. *J. Catal.* **2003**, *214*, 78. https://doi.org/10.1016/S0021-9517(02)00081-7
25. Li, R.; Yao, W.; Jin, Y.; Jia, W.; Chen, X.; Chen, J.; Zheng, J.; Hu, Y.; Han, D.; Zhao, J. *Chem. Eng. J.* **2018**, *351*, 995. https://doi.org/10.1016/j.cej.2018.06.146
26. Mironenko, R. M.; Belskaya, O. B.; Likholobov, V. A. *Catal. Today* **2020**, *357*, 152. https://doi.org/10.1016/j.cattod.2019.03.023
27. Ryndin, Yu. A.; Alekseev, O. S.; Simonov, P. A.; Likholobov, V. A. *J. Mol. Catal.* **1989**, *55*, 109. https://doi.org/10.1016/0304-5102(89)80247-0
28. Dlamini, M. W. Ph.D. Thesis, University of the Witwatersrand: Johannesburg, South Africa, 2016.
29. Shin, Y.-R.; Jung, S.-M.; Jeon, I.-Y.; Baek, J.-B. *Carbon* **2013**, *52*, 493. https://doi.org/10.1016/j.carbon.2012.10.001
30. Manikai, S. M.Ph.D. Thesis, University of the Witwatersrand: Johannesburg, South Africa, 2015.
31. Jiang, F.; Cai, J.; Liu, B.; Xu, Y.; Liu, X. *RSC Adv.* **2016**, *6*, 75541. https://doi.org/10.1039/C6RA17000E
32. Zhang, L.; Winterbottom, J. M.; Boyes, A. P.; Raymahasay, S. *J. Chem. Technol. Biotechnol.* **1998**, *72*, 264. https://doi.org/10.1002/(SICI)1097-4660(199807)72:3%3C264::AID-JCTB897%3E3.0.CO;2-2
33. Cabiac, A.; Cacciaguerra, T.; Trens, P.; Durand, R.; Delahay, G.; Medevielle, A.; Plée, D.; Coq, B. *Appl. Catal. Gen.* **2008**, *340*, 229. https://doi.org/10.1016/j.apcata.2008.02.018
34. Cattaneo, S.; Sanchez Trujillo, F. J.; Dimitratos, N.; Villa, A. *Appl. Sci.* **2019**, *9*, 5061. https://doi.org/10.3390/app9235061
35. Vatti, S. K.; Krishnamurthy, K. K. R.; Viswanathan, B. *Chemrxiv*, **2020**.

https://doi.org/10.26434/chemrxiv.12964598.v1